

# The Effect of Nuclear Shape

S.E. Chernyshev and K.V. Shitikova \*

(August 31, 2018)

## Abstract

The effect of projectile shape on cross sections and momentum distributions of fragments from heavy ion reactions is studied. We propose a new approach that implements the underlying symmetries of each isotope with a few parameters directly in the density. Various densities and their nuclear structure are then analyzed in the reactions of  $^{12}\text{C}$  and  $^{11}\text{Li}$ ,  $^{11}\text{Be}$ , and  $^{11}\text{C}$  on a carbon target.

PACS numbers: 21.10.Gv, 21.60.-Fw, 25.60.+v, 25.70.Mn, 25.75.+r

Typeset using REVTeX

---

\*Permanent address: Institute for Nuclear Physics, Moscow State University, 119899, Moscow, Russia

## I. INTRODUCTION

In a previous paper [1] in reactions of  $^{12}\text{C}$  and  $^{11}\text{Li}$  projectiles on a  $^{12}\text{C}$  target, it has been shown that the total reaction cross section, inclusive fragment cross sections and fragment momentum distributions are sensitive to the assumed proton and neutron radial density distributions of the projectile. These results stimulated us to further investigate effects of nuclear shape of neutron rich isotopes in the heavy ions reactions. A special attention in our investigations will be given to the neutron halo nuclei for the following reason. Recent developments of radioactive nuclear beams enabled one to study a detailed structure of nuclei far from the stability line [2]. The neutron halos have been observed in nuclei near the neutron drip line by reaction measurements with intermediate and high energy radioactive nuclear beams. These nuclei are of a special interest in relation to shell structures near the drip line and to new excitation modes associated with the excess neutron on the nuclear surface.

In this paper we use the method of hyperspherical functions (HSF) [3] to construct the densities of the light drip line nuclei. Such nuclei typically have small binding energies and extended radial densities, and for them a suitable treatment of the tails of nuclear radial wave functions is essential. Physically such wave functions should have exponential tails. A main advantage of the HSF is that it provides a realistic radial wave functions at large distances. In addition, the spurious center-of-mass motion is removed from the onset and the symmetries are properly taken into account. In [4], an attempt was made to provide a unified description of  $^{6,7,8,9,11}\text{Li}$  rather than just a single isotope. Instead of trying to parameterize the effective interaction for each isotope, a simple parametrization for all the isotopes is used. Furthermore, there is no inert core and all the nucleons are properly antisymmetrized. Finally, because Jacobian coordinates are used, no problems are encountered with the treatment of the center of mass. The binding energy of a nucleus serves as a natural scale in this approach and is related to all other observables.

In order to account for the clusterization effect more precisely in our calculations, we ex-

pand the HSF in the translationally invariant many body harmonic oscillator (HO) functions [5] and implement the nuclear structure straight in the densities. We use a few one-body oscillator parameters in order to better reproduce the experimentally observed mean-square radii (rms) and density distributions. These densities are then used in Monte Carlo simulations of nucleon-nucleon collisions, in which the total and inclusive cross sections and transverse momentum distributions of fragments are calculated. Thoroughly tested, this approach gives a clear picture of nuclear shape.

The paper is organized as follows. In Section II, the HSF method is described. Next we elaborate on the details of the expansion with respect to the radial wave functions of a  $(3A-3)$ -dimensional harmonic oscillator. In Section III, we give a brief summary of the light isotopes and construct their Young diagrams. Knowing the underlying symmetries, we first build the "normal"  $^{12}\text{C}$  density and compare it with other approximations. We calculate the elastic form-factor and run a  $^{12}\text{C} + ^{12}\text{C}$  simulation to see how it works in a standard case. Armed with the results, we proceed to the neutron rich  $^{11}\text{Li}$  and also  $^{11}\text{Be}$ ,  $^{11}\text{C}$  for comparison. In order to make the paper more coherent, we include all the densities in Section III and analyze the reactions in Section IV. The results are in reasonable agreement with experiment and other theoretical approaches. Our conclusions are summarized in section V.

## II. METHOD OF THE HYPERSPHERICAL FUNCTIONS

The HSF method involves a collective variable (hyperradius  $\rho$ ) which is related to the mean-square radius of the nucleus  $\rho^2 = A \langle r^2 \rangle$ , i.e., to the mean nuclear density. The excitations of this degree of freedom correspond to the monopole oscillation of the nucleus as a whole and thus the density can be treated as dynamic variable.

The wave function  $\Psi$  of a nucleus with  $A$  nucleons is translationally invariant and depends on the  $x_1, x_2, \dots, x_{A-1}$  Jacobi coordinates, defined as

$$x_1 = \sqrt{\frac{1}{2}}(\mathbf{r}_1 - \mathbf{r}_2)$$

$$\begin{aligned}
x_2 &= \sqrt{\frac{2}{3}} \left[ \frac{1}{2} (\mathbf{r}_1 + \mathbf{r}_2) - \mathbf{r}_3 \right] \\
&\vdots \\
x_{A-1} &= \sqrt{\frac{A-1}{A}} \left[ \frac{1}{A-1} \sum_{i=1}^{A-1} \mathbf{r}_i - \mathbf{r}_A \right]
\end{aligned} \tag{1}$$

Here  $\mathbf{r}_i$  is the coordinate of the  $i$ -th nucleon. Each coordinate is a distance between the  $(i+1)$ -th nucleon and the center of mass of the groups of nucleons  $1, 2, \dots, i$ . The hyperspherical coordinates (hyperradius  $\rho$  and  $(3A-4)$  hyperspherical angles) are chosen as

$$\begin{aligned}
x_1 &= \rho \sin \theta_{n-1} \dots \sin \theta_2 \sin \theta_1 \\
x_2 &= \rho \sin \theta_{n-1} \dots \sin \theta_2 \cos \theta_1 \\
&\vdots \\
x_{n-1} &= \rho \sin \theta_{n-1} \cos \theta_{n-2} \\
x_n &= \rho \cos \theta_{n-1} \\
\rho^2 &= \sum_{i=1}^n x_i^2 \quad 0 \leq \rho \leq \infty \\
0 \leq \theta_1 &\leq 2\pi, \quad 0 \leq \theta_k \leq \pi \quad k > 1
\end{aligned} \tag{2}$$

for  $n = 3(A-1)$ -dimensional space of the Jacobi coordinates. For this set of coordinates, the volume element  $dV$  reads

$$dV = dx_1 dx_2 \dots dx_n = \rho^{n-1} d\rho d\Omega \tag{3}$$

where the solid angle element  $d\Omega$  is

$$d\Omega = \sin^{n-2} \theta_{n-1} \sin^{n-3} \theta_{n-2} \dots \sin \theta_2 d\theta_{n-1} d\theta_{n-2} \dots d\theta_1 \tag{4}$$

The Laplacian is given by

$$\begin{aligned}
\Delta_n &= \sum_n \frac{\partial^2}{\partial x_n^2} = \frac{1}{\rho^{n-1}} \frac{\partial}{\partial \rho} \left( \rho^{n-1} \frac{\partial}{\partial \rho} \right) + \frac{1}{\rho^2} \Delta_{\Omega_n} \\
\Delta_{\Omega_n} &= \frac{1}{\sin^{n-2} \theta_{n-1}} \frac{\partial}{\partial \theta_{n-1}} \left( \sin^{n-2} \theta_{n-1} \frac{\partial}{\partial \theta_{n-1}} \right) + \frac{1}{\sin^2 \theta_{n-1}} \Delta_{\Omega_{n-1}}
\end{aligned} \tag{5}$$

The hyperspherical functions, or  $K$ -harmonics, are the eigenfunctions of the angular part of the Laplacian

$$\Delta_{\Omega_n} Y_{K\gamma}(\theta_i) = -K(K + n - 2)Y_{K\gamma}(\theta_i). \quad (6)$$

The value of  $K$  is the analog of the angular momentum at  $n = 3$  and is called the global momentum. The subscript  $\gamma$  denotes all the quantum numbers necessary to enumerate the various degenerate states of Eq. (6). For  $\gamma$  it is expedient to use the Young diagram  $[f]$  and the Yamanouchi symbol  $(r)$ , characterizing the  $K$ -harmonics properties relative to the  $A$ -nucleon permutations, and  $LST$  to designate the orbital momentum, spin and isospin of this state.

The wave function of a nucleus is then expressed in the form of an expansion in the  $K$ -harmonic polynomials [6]

$$\begin{aligned} \Psi(1, 2 \dots A) &= \rho^{-(3A-4)/2} \sum_{K\gamma} \chi_{K\gamma}(\rho) Y_{K\gamma}(\theta) \\ \int_0^\infty \chi_{K\gamma}^2(\rho) d\rho &= 1 \quad \gamma = [f]rLST \end{aligned} \quad (7)$$

The Hamiltonian reads

$$\mathcal{H} = -\frac{\hbar^2}{2m} \frac{1}{\rho^{3A-4}} \frac{\partial}{\partial \rho} \left( \rho^{3A-4} \frac{\partial}{\partial \rho} \right) - \frac{\hbar^2}{2m} \frac{\Delta_{\Omega}}{\rho^2} + V \quad (8)$$

Here  $m$  is the mass of a nucleon. The Schroedinger equation for the radial function  $\chi_{K\gamma}(\rho)$  can be written as

$$\left\{ \frac{d^2}{d\rho^2} - \frac{L_K(L_K + 1)}{\rho^2} - \frac{2m}{\hbar^2} [\mathcal{E} + W_{K\gamma}^{K\gamma}(\rho)] \right\} \chi_{K\gamma}(\rho) = \frac{2m}{\hbar^2} \sum_{K'\gamma' \neq K\gamma} W_{K\gamma}^{K'\gamma'}(\rho) \chi_{K'\gamma'}(\rho) \quad (9)$$

where  $L_K = K + (3A - 6)/2$ , and  $W_{K\gamma}^{K'\gamma'}(\rho)$  are the matrix elements of the nucleon-nucleon interaction

$$V = \sum_{i < j}^A V(r_{ij}) \quad V(r_{ij}) = f(r_{ij}) W_{\sigma\tau} \quad (10)$$

which may be expressed through the two-body fractional parentage coefficients in the form

$$\begin{aligned}
W_{K\gamma}^{K'\gamma'}(\rho) &= \langle AK[f]rLSTM_L M_S M_T | \hat{V} | AK'[f]r'L'S'T'M_L M_{S'} M_{T'} \rangle \\
&= \frac{A(A-1)}{2} \sum_{K_2, \gamma_2} \langle AK[f]rLST | (A-2)K_2[f]r_2 L_2 S_2 T_2 \Lambda(L''K''); L_0 S_0 T_0 \rangle \\
&\times \langle S_0 T_0 | W_{\sigma\tau} | S_0 T_0 \rangle R_{K''L_0}^{KK'}(\rho) \\
&\times \langle (A-2)K_2[f]r_2 L_2 S_2 T_2 \Lambda(L''K''); L_0 S_0 T_0 | AK'[f]r'L'S'T' \rangle
\end{aligned} \tag{11}$$

Here

$$\begin{aligned}
R_{K''L_0}^{KK'}(\rho) &= \int d\theta_1 \sin^{3A-7} \theta_1 \cos^2 \theta_1 \mathcal{N}_{KK''L_0} \mathcal{N}_{K'K''L_0} \\
&\times f(\rho \cos \theta_1) \sin^{2K''} \cos^{2L_0} \theta_1 P_{K-K''-L_0}^{K''+(3A-6)/2-1, L_0+1/2}(\cos 2\theta_1) \\
&\times P_{K'-K''-L_0}^{K''+(3A-6)/2-1, L_0+1/2}(\cos 2\theta_1)
\end{aligned} \tag{12}$$

$\langle S_0 T_0 | W_{\sigma\tau} | S_0 T_0 \rangle$  is the spin-isospin part of the interaction matrix element. The collective potential  $W_{K\gamma}^{K'\gamma'}(\rho)$  is given by integrals containing two-body matrix elements together with the  $K$ -harmonics fractional parentage coefficients. In the previous investigations [7] it was shown that with the HSF one may use the same formulas for the fractional parentage coefficients which were obtained earlier with the translationally invariant shell model. In this case the Talmi-Moshinsky coefficients must be replaced by the Raynal-Revai coefficients, 6j-symbols must be added for the over-binding of the global momentum  $K$ , and additional phase multipliers are inserted. Their use has led to a significant improvement of the computations [8]. The calculation is simplified if only the first few terms in the expansion (7), i.e.,  $K = K_{min}$  and  $K = K_{min} + 1$  are taken into account. Usually one adopts the  $K_{min}$  approximation in which all values of  $K$  greater than  $K_{min} = A - 4$  ( $A \leq 16$ ) are neglected. The success of this approximation lies in the fact that the centrifugal barrier reduces the contributions of configurations with  $K$  greater than  $K_{min}$  in the equations determining the hyperspherical wave functions.

## A. Expansion

The system (9) has an analytical solution for the harmonic oscillator potential  $V = m\omega^2 \rho^2 / 2$  [7]. The energy eigenvalues are given by

$$\mathcal{E}_\nu = (2\nu + K + \frac{n}{2}) \hbar\omega \quad (13)$$

with the eigenfunctions

$$\mathcal{R}_{\nu K}(x) = \sqrt{\frac{2\nu!}{\Gamma(\nu + K + \frac{n}{2})}} e^{-\frac{1}{2}x^2} x^K L_\nu^{K+\frac{1}{2}(n-2)}(x^2) \quad (14)$$

where we have introduced a dimensionless parameter  $x = \rho/r_0$  with  $r_0^2 = \hbar/m\omega$  and the associated Laguerre polynomials are defined as

$$L_n^\alpha(x) = \sum_{k=0}^n (-1)^k \frac{(n+\alpha)!}{(n-k)!(k+\alpha)!k!} x^k \quad (15)$$

Let us briefly examine critical regimes for the Schroedinger equation (9). As  $\rho \rightarrow 0$ , it is reduced to

$$\frac{d^2}{d\rho^2}\chi(\rho) = \frac{L_K(L_K + 1)}{\rho^2}\chi(\rho) \quad (16)$$

with the trivial eigenfunction

$$\chi(\rho) \sim \rho^{L_K+1} \quad (17)$$

On the other hand, as  $\rho \rightarrow \infty$ , the Eq. (9) reads

$$\frac{d^2}{d\rho^2}\chi(\rho) = \frac{2mE}{\hbar^2}\chi(\rho) \quad (18)$$

and the eigenfunction has the following asymptotical behavior

$$\chi(\rho) \sim \exp\left(-\sqrt{\frac{2mE}{\hbar^2}} \rho\right) \quad (19)$$

as was mentioned in the Introduction. We will return to this important point in next the section.

Now we can express radial functions  $\chi_K^\gamma(\rho)$  in terms of the  $3(A-1)$ -dimensional harmonic oscillator, as shown on Figure 1 for the  $^{12}\text{C}$  nucleus,

$$\chi_K^\gamma(\rho) = \sum_\nu C_{\nu K}^\gamma R_{\nu K}(\rho) \quad (20)$$

and the expansion coefficients are given by

$$C_{\nu K}^\gamma = \int \chi_K^\gamma(\rho) R_{\nu K}(\rho) \rho^{\frac{1}{2}(3A-4)} d\rho \quad (21)$$

$$C_0 \simeq 0.984, \quad C_1 \simeq -0.061,$$

$$C_2 \simeq 0.158, \quad C_3 \simeq 0.055.$$

with the oscillator frequency  $\hbar\omega$  determined so that the maximum of the lowest oscillator function  $R_{0K}(\rho)$  coincides with the maximum of the lowest hyperspherical function  $\chi_K^0(\rho)$ . We will deal only with the ground state wave function and use  $C_{\nu K_{min}}^0 = C_\nu$  for short.

It is striking that the overlap integral of the ground state radial function  $\chi_K^0(\rho)$  with the lowest oscillator function  $R_{0K}(\rho)$  is 98%. At the same time, the contribution to  $\chi_K^0(\rho)$  of the two-quantum oscillator excitation is exceptionally small. A very small value of the coefficient  $C_1$  is not fortuitous but conforms to the theorem [9], which states that if the oscillator frequency  $\hbar\omega$  is chosen to make the overlap integral of  $R_{0K}(\rho)$  and  $\chi_K^0(\rho)$  maximal, then the overlap integral of  $\chi_K^0(\rho)$  with  $R_{1K}(\rho)$  is strictly zero.

As we have already noted, in choosing  $\hbar\omega$  we did not achieve a maximum value of the  $\chi_K^0(\rho)$ ,  $R_{0K}(\rho)$  overlap, but assured only a coincidence of the maxima of these functions. However, if such a condition is satisfied, the overlap integral of the functions is fairly near the maximum, and the coefficient  $C_1$  is very small, although nonvanishing. This circumstance casts light on the origin of close agreement between the results of the translationally invariant shell model and the HSF method for the ground state. Since the function  $R_{1K}(\rho)$  cannot be mixed with  $R_{0K}(\rho)$ , the shell function in the HSF method is improved by admixture of states with oscillator energy  $4\hbar\omega$  and higher. Because of the large difference between the energies of these states and the ground state, this admixture is small.

Then one can derive the binding energy as a function of the interaction matrix elements

$$\begin{aligned} E_{\nu K} &= \frac{1}{2}\hbar\omega \left( 2\nu + \frac{5A-11}{2} \right) \\ &+ \frac{1}{2}\hbar\omega \left[ \frac{C_{\nu+1}}{C_\nu} \sqrt{(\nu+1)\left(\nu + \frac{5A-11}{2}\right)} + \frac{C_{\nu-1}}{C_\nu} \sqrt{\nu\left(\nu + \frac{5A-13}{2}\right)} \right] \\ &+ \sum_\mu \frac{C_\mu}{C_\nu} \int R_{\nu K}(\rho) W_{K\nu}^{K\mu}(\rho) R_{\mu K}(\rho) \rho^{3A-4} d\rho \end{aligned} \quad (22)$$



The rms of a nucleus is given by

$$\langle \bar{r}^2 \rangle_\nu = \frac{\hbar}{m\omega} \frac{1}{A} \left[ \sum_\nu C_\nu C_\nu (2\nu + \frac{5A-11}{2}) - 2 \sum_\nu C_\nu C_{\nu+1} \sqrt{(\nu+1)(\nu + \frac{5A-11}{2})} \right] \quad (23)$$

### III. SYMMETRIES OF NEUTRON RICH ISOTOPES

Using the Young-Yamanouchi classification scheme [10], which stems from the orthogonal representation of a given permutation group, and with the knowledge of the total spin and isospin of the nucleus, we determine the symmetry with a corresponding Young diagram [ $f$ ] of each isotope. In Table I results of the classification of  ${}^6\text{-}^{13}\text{Li}$ ,  ${}^6\text{-}^{12}\text{Be}$ ,  ${}^7\text{-}^{13}\text{B}$  (for completeness), and  ${}^8\text{-}^{14}\text{C}$  nuclei are collected. The Lithium sequence, illustrated in Figure 2, reflects the strong excitation in the isospin. The neutron super-rich  ${}^{13}\text{Li}$  obtains an extra pair of halos in the same manner as  ${}^{11}\text{Li}$  results from  ${}^9\text{Li}$  by adding two halo neutrons. In the brackets we have put two possible versions of a transitory  ${}^{10}\text{Li}$  state.

Note that while for the most part these sequences are rather straightforward, obtained by a simple adding of a neutron to the p-shell, some isotopes like  ${}^{11}\text{Be}$  do stand out. There has been a great deal of interest in the effect of clusterization, and our scheme seems to agree with a recent study of the multi-cluster structure [11], that a simple description in terms of one Young diagram may not be adequate for some isotopes.

Having thus established the symmetry requirements on the neutron content of different isotopes, we proceed to construct the density distributions for the light nuclei. Originally, this classification was applied to the construction of the HSF wave functions [4]. In Table II we reproduce their results for the binding energy and rms for  ${}^6\text{-}^{11}\text{Li}$  and  ${}^{11}\text{C}$  isotopes in comparison with the experimental data. It can be seen that the variation in the binding energy as a function of the mass number and rms for the Lithium isotopes is qualitatively reproduced. A comparison of  ${}^{11}\text{Li}$  and  ${}^{11}\text{C}$  shows a very strong nuclear structure effect on the binding energy and rms.

If one would like to look at the more detailed description of the nuclear structure which comes with the wave function and exhibits the nuclear shape through the nuclear densities,

one may use the information that comes from measurements of the total reaction cross sections and the inclusive cross sections for fragments in which the projectile has lost one neutron or proton. In Ref. [1] it has been shown that both the cross sections and the fragment momentum distributions lead to the conclusion that the HSF density distributions in the  $K_{min}$  approximation extend too far for protons and not far enough for neutrons. The inclusion of several more terms in the expansion (7) will give an extension of the asymptotic density to larger radii. This will give better agreement between the HSF method and the experimental data. For this reason we propose another approach in which the clusterization effect is taken into account directly in the density.

### A. Density

From the formulae in section II one derives the density of nuclear matter through

$$n_{J^\pi J'^{\pi'}}(\mathbf{r}) = \left\langle J^\pi \left| \sum_K \delta(\mathbf{r} - \mathbf{r}_K) \right| J'^{\pi'} \right\rangle \quad (24)$$

with

$$n_{J^\pi J'^{\pi'}}(\mathbf{r}) = \sum_{\lambda\mu} n_{J^\pi J'^{\pi'}}^\lambda(r) Y_{\lambda\mu}(\theta, \phi) \quad (25)$$

and the radial component is expressed as

$$n_{J^\pi J'^{\pi'}}^\lambda(\mathbf{r}) = \left\langle J^\pi \left| \sum_K \mathbf{r}_k^{-2} \delta(\mathbf{r} - \mathbf{r}_K) Y_{\lambda\mu}(\theta, \phi) \right| J'^{\pi'} \right\rangle \quad (26)$$

The radial density distribution reads ( $A \leq 16$ ) [8]

$$\begin{aligned} n_{ij}(r) &= \frac{16}{\sqrt{\pi}} \frac{\Gamma\left(\frac{1}{2}(5A-11)\right)}{\Gamma\left(\frac{1}{2}(5A-14)\right)} \int_r^\infty \frac{(\rho^2 - r^2)^{\frac{1}{2}(5A-16)}}{\rho^{5A-13}} \chi_i(\rho) \chi_j(\rho) d\rho \\ &+ \frac{8}{3} \frac{A-4}{\sqrt{\pi}} \frac{\Gamma\left(\frac{1}{2}(5A-11)\right)}{\Gamma\left(\frac{1}{2}(5A-16)\right)} \int_r^\infty \frac{r^2 (\rho^2 - r^2)^{\frac{1}{2}(5A-18)}}{\rho^{5A-13}} \chi_i(\rho) \chi_j(\rho) d\rho \end{aligned} \quad (27)$$

with the s-shell (first line) and p-shell densities explicitly shown. We also treat the halo neutrons  $N_h$  separately from the p-shell nucleons. The rms of each shell is calculated as

$$\langle r_{ii}^2 \rangle_{shell} = \frac{\int n_{ii}^{shell}(r) r^4 dr}{\int n_{ii}^{shell}(r) r^2 dr} \quad (28)$$

with the density normalization

$$4\pi \int_0^\infty n_i^{(s,p,h)}(r) r^2 dr = (4, A - 4 - N_h, N_h) \quad (29)$$

Before calculating the densities for the neutron rich isotopes, we would like to check on a standard nucleus such as  $^{12}\text{C}$ , for which there exist a few other density approximations.

- In Ref. [12] the exact HSF density for  $^4\text{He}$ ,  $^6\text{Li}$ ,  $^{12}\text{C}$ , and  $^{16}\text{O}$  was approximated by

$$n(r) = \sum_{i=0}^k a_i \frac{r^{2i}}{r_i^{2i}} e^{-r^2/r_i^2} \quad (30)$$

motivated by the analogy with the harmonic oscillator. Using different oscillator parameters  $a_i$ ,  $r_i$ , one could easily fit various experimental observables, such as the rms and so on. For the ground state of  $^{12}\text{C}$ , it was enough to have the first two terms

$$n(r) = a_s e^{-r^2/r_s^2} + a_p \frac{r^2}{r_p^2} e^{-r^2/r_p^2} \quad (31)$$

with  $r_s = 2.0$  fm,  $r_p = 1.7$  fm and  $a_s = 0.718348$ ,  $a_p = 0.957798$  fixed to the normalization of 4 s-shell and 8 p-shell nucleons.

- Harvey used a phenomenological approach [13] to obtain the densities for  $^{12}\text{C}$  and  $^{11}\text{Li}$ . Since the Monte Carlo simulations require a separate density distribution for nucleons with different binding energies, a harmonic oscillator model was used for projectiles and a standard Fermi shape for the  $^{12}\text{C}$  target. For example, for  $^{11}\text{Li}$  the  $s$ -shell parameter was chosen to be 1.619 fm for protons and neutrons, and for the  $p$ -shell 2.0 fm for protons and 2.1 fm for neutrons. It was also assumed that there was one proton and four neutrons in the  $p_{3/2}$ -shell. The outer two neutrons were assumed to have an exponential density distribution beyond a radius of 2.5 fm

$$n(r) = 0.3323 \frac{e^{-2r/L}}{r^2} \quad (32)$$

with  $L=3.7$  fm. As we mentioned above, the HSF functions have an exponential asymptotics (19) and thus become very attractive from a phenomenological point of view. The normalization, 0.3323, came from the requirement that the volume integral contain just two neutrons. The values of the harmonic oscillator parameters and of  $L$  were chosen to fit the experimental reaction cross section and the  ${}^9\text{Li}$ ,  ${}^8\text{He}$  inclusive cross sections for the reaction  ${}^{11}\text{Li}+\text{C}$  at 790 MeV/A.

- Returning to the HSF method, one does not have as much freedom in choosing various parameters. It is very important that in the HSF one obtained a self-adjusted system in which the parameters of the interaction determine the size of the system. However, working in the  $K_{min}$  approximation, one needs to improve the neutron density asymptotics. Having derived the explicit formula (27) for the density distribution and knowing the symmetry requirements on the neutron content of different isotopes, we are now in the position to do it directly in the density.

Since the wave function characterizes the nucleus as a whole, the binding energy  $E_{0K}$ , cf. Eq. (22), sets its scale  $r_A = \hbar/m\omega$ . It also serves as a natural parameter for the s-shell, the core of a nucleus. The p-shell basically carries all the information about a given isotope, and its scale will be chosen so that experimental rms is reproduced. In accordance with our group-theoretical framework, another parameter will be used for the halo neutrons, still fitting to the experimental rms.

For example, the p-shell density then reads

$$n_{ij}^p(r) = \frac{8}{3} \frac{A-4}{\sqrt{\pi}} \frac{\Gamma\left(\frac{1}{2}(5A-11)\right)}{\Gamma\left(\frac{1}{2}(5A-16)\right)} \int_r^\infty \frac{r'^2 (\rho_p'^2 - r'^2)^{\frac{1}{2}(5A-18)}}{\rho_p'^{5A-13}} \chi_i(\rho_A) \chi_j(\rho_A) d\rho_p' \quad (33)$$

with scaling

$$\rho_p \rightarrow \frac{\rho}{r_p} \quad \rho_A \rightarrow \frac{\rho}{r_A} \quad (34)$$

Table III shows the parameters for these densities, the rms for each shell and of the nucleus as a whole. They reproduce the experimental radii of Tanihata, et al. [2,14]. In

Figure 3 we plot the densities for  $^{12}\text{C}$  and  $^{11}\text{Li}$ . The  $^{11}\text{Li}$  one is in reasonable agreement with the shaded region of the experimental density [15].

### B. Charged form-factors

Having obtained the total densities, one can quickly probe its charge distribution by looking at the elastic  $e^-$  scattering off that nucleus, or its charged form-factor. For a nucleus with  $Z$  protons it may be written in the Born approximation as

$$F_{ch}(q) = f_p(q) f_{CM}(q) \frac{1}{Z} F_z(q) \quad (35)$$

with the elastic point-proton form-factor  $F_z(q)$  defined as

$$F_z(q) = 4\pi \int_0^\infty n_z(r) \frac{\sin(qr)}{qr} r^2 dr \quad (36)$$

where  $n_z(r)$  is the proton part of the total density. The correction for the center of mass motion  $f_{CM}(q)$  is not required in our approach since it is factorized from the very beginning (cf. Eq. 9).  $f_p(q)$  is the correction for the finite proton size, which we take to be

$$f_p(q) = [1 + q^2/q_0^2]^{-2} \quad (37)$$

with  $q_0 = 4.33 \text{ fm}^{-1}$  corresponding to  $r_{rms} = 0.8 \text{ fm}$  for the proton.

In Figure 4 we plot the charged form-factors for  $^6\text{Li}$  and  $^{12}\text{C}$  with the data points taken from [16,17], where for the momentum axis a standard  $q_{eff}$  is used

$$q_{eff} = q \left[ 1 + \frac{4Z\alpha\hbar c}{3r_{rms}E_0} \right] \quad (38)$$

Note, that the elastic rms radii for these nuclei are different from the reaction ones [2], and we have slightly modified our parameters so that their densities reproduce the observed  $r_{rms}(^6\text{Li}) = 2.56 \text{ fm}$  and  $r_{rms}(^{12}\text{C}) = 2.48 \text{ fm}$ . Our results match well the minima of the experimental form-factors and qualitatively follow their shape. They also compare favorably with the full HSF calculation [4,18].

Having determined all the parameters in the density, we are ready to analyze the reactions.

## IV. MONTE CARLO AND NUCLEAR SHAPE

The Monte Carlo method allows the calculation of cross sections and momentum distributions of primary fragments arising from nucleon-nucleon collisions between a target and a projectile at energies above 200 MeV/nucleon. The primary fragments may subsequently decay to the final observed nuclei.

This method has been shown [19] to give results in good agreement with experiment for the total reaction cross section, fragment inclusive cross sections, fragment exclusive (coincidence channel) yields, fragment momenta, both inclusive and in different coincidence channels. It is also possible to calculate the momentum distributions of nucleons that are either knocked out of the projectile or come from the subsequent decay. Thus, unlike many theoretical techniques, the Monte Carlo decay method permits the comparison of calculated and experimental values for essentially all the measured quantities and allows to test radial density distributions derived from various theoretical models. The purpose of the present work is therefore to compare experimental values with those obtained from the HSF density distributions with the aim to get the maximum of information about nuclear shape.

### A. $^{12}\text{C} + ^{12}\text{C}$

When one or two neutrons are lost in a collision between the projectile with a diffuse neutron rich surface and a target nucleus, the transverse momentum distribution of the fragments thus produced can be fit with a double Gaussian curve in which a narrow component is superimposed on a much broader one [13]. This phenomenon is also observed for fragments from the normal projectile  $^{12}\text{C}$ . The shape of the fragment momentum distribution is sensitive to the assumed projectile surface diffusivity. As the surface diffusivity increases, the width of the broad component decreases. For the sharp cutoff shape, the distribution has no narrow component.

The study of the nuclear structure effect in  $^{12}\text{C} + ^{12}\text{C}$  scattering, using the optical

model [20] and the calculation of the total reaction cross sections in the Glauber model [21] convincingly show that the total reaction cross sections are sensitive to the form of the density. With that in mind, we have conducted the Monte Carlo simulations with three different densities: minimal  $n(R_{0K})$ , obtained with  $R_{0K}$  instead of the full function  $\chi$  of Eq. (20),  $n(\chi)$  and the approximation of Eq. (31). The experimental data and our results are collected in Table IV. As expected, the total cross sections did not vary much, since we had the same  $r_{rms}$  for each density distribution.

The tail effect is deduced from the momentum distribution of  $^{11}\text{C}$  fragments. In a fit with the double Gaussian curve, the narrow component reflects the behavior of the tail of the density and thus we see that having all four functions of the Eq. (20) decomposition improves the resulting width of both narrow and broad components as compared to the minimal  $n(R_{0K})$  density.

In Figure 5 we fit the transverse momentum distribution of the  $^{11}\text{C}$  fragments from our  $n(\chi)$  density with one and two Gaussian curves. One Gaussian fit is quite reasonable and gives a very close  $\sigma_B = 103$  to the experimental  $\sigma_B = 105$ . Overall, our numbers match well with the experimental data and phenomenological results of Ref. [13].

Having thus convinced ourselves that this approach works well for the standard nucleus, we turn to the reactions with the neutron rich isotopes as projectiles on the carbon target.

## B. $^{11}\text{Li} + ^{12}\text{C}$

In analyzing this reaction, we emphasize the halo effect. The momentum distribution of  $^9\text{Li}$  fragments from  $^{11}\text{Li} + \text{C}$  at 790 MeV/c has been experimentally studied [22]. It has broad and narrow Gaussian components with widths of 80 and 21 MeV/c and a ratio of areas B/N of 1.5. Since the shape of the momentum distribution is sensitive to the projectile surface diffusivity, we have used two different HSF densities with a very loose pair of halo neutrons  $n(^{11}\text{Li}_h)$  and another one  $n(^{11}\text{Li}_p)$  by placing them relatively close to the p-shell. The results for  $n(^{11}\text{Li}_h)$  are shown in Figure 6 and the rest is summarized in Table V. While

the width of the broad component is well reproduced, the narrow component is too wide, especially for  $n(^{11}\text{Li}_p)$ . This result is consistent with the absence of a long neutron ‘tail’ at large radii and low local neutron densities which give a small value for the local Fermi momentum. A short tail also manifests itself in the somewhat low total cross sections, which drops even more for  $n(^{11}\text{Li}_p)$ . This indicates that the halo pair gives a major contribution to the neutron tail and has an unusually large rms radius. We would like to point out that our result  $\sqrt{\langle r^2 \rangle_o} \sim 5.23 \text{ fm}$  for an outer pair of halo neutrons for  $n(^{11}\text{Li}_h)$  is consistent with experimental  $4.8 \pm 0.8 \text{ fm}$  [15] and  $5.1_{-0.9}^{+0.6} \text{ fm}$  [23].

At last, we would like to analyze the structure effect by comparing  $^{11}\text{Li}$ ,  $^{11}\text{Be}$ , and  $^{11}\text{C}$ , which have the same number of nucleons but different Young diagrams. From  $^{11}\text{C}$  with  $[f] = [443]$  and isospin  $T = 1/2$ , one sees the increase in the isospin in  $^{11}\text{Be}$  with  $[f] = [4331]$ ,  $T = 3/2$  to  $^{11}\text{Li}$  with  $[f] = [4322]$ ,  $T = 5/2$ . Their cross sections, see Table VI, vividly show this change in their nuclear structure. Starting with  $\sigma_{^{11}\text{C}} = 880 \text{ mb}$ , the cross section jumps to  $\sigma_R = 946 \text{ mb}$  for  $^{11}\text{Be}$ , indicating some sort of a halo neutron tail and culminates in  $\sigma_{^{11}\text{Li}} = 994 \text{ mb}$  with two halo neutrons. It unambiguously verifies that our approach correctly implements the underlying symmetries of each isotope and works well with a judicious choice of parameters directly in the density level, bypassing the parameters of the nucleon-nucleon interaction.

## V. CONCLUSION

The hyperspherical functions method provides a convenient basis for the description of the neutron rich isotopes. The underlying symmetry of each isotope exhibits a simple structure and reproduces the clusterization effect. Studies of the reaction cross section and the inclusive cross sections for fragments in which the projectile has lost one neutron or one proton give a powerful method for investigating the neutron, proton and total densities in the surface of the projectile. Here we have proposed a new approach which takes into account the clusterization effect directly to the densities of the drip line nuclei.



## ACKNOWLEDGMENTS

We would like to express our deep gratitude to Prof. B.G. Harvey for many useful discussions and great help with the Monte Carlo part of the calculations. One of the authors gratefully acknowledges the hospitality of the Nuclear Theory Group at Stony Brook. This work was supported in part by the Department of Energy under Grant No. DE-FG02-88ER40388.

## REFERENCES

- [1] B.G. Harvey, K.V. Shitikova, G.D. Yen, *The Effect of Projectile Shape*, Keywest Proceedings, (1995).
- [2] I. Tanihata, et al. Phys. Lett. **B160**, 380 (1985); Phys. Rev. Lett. **55**, 2676 (1985).
- [3] R.I. Dzhibuti and K.V. Shitikova, *Method of Hyperspherical Functions in Atomic and Nuclear Physics*, M. Energoatomizdat, (1993) (in Russian).
- [4] V.V. Burov, et al, Phys. Atom. Nucl. **57**, 2095 (1994).
- [5] K.V. Shitikova, Nucl. Phys. **A 331**, 365 (1979).
- [6] Yu.A. Simonov, Sov. J. Nucl. Phys. **3**, 630 (1966).
- [7] Yu.F. Smirnov and K.V. Shitikova, Sov. J. Part. Nucl. **8**, 847 (1977).
- [8] R.I. Dzhibuti and K.V. Shitikova, Sov. J. Part. Nucl. **20**, 331 (1989).
- [9] M. Dubovoy and J. Flores, Rev. Mex. Phys. **17**, 289 (1968).
- [10] H.A. Jahn and H. Van Wieringen, Proc. Roy. Soc. **A 209**, 502 (1951).
- [11] Y. Suzuki, et al, Preprint N9601, nucl-th/9604020.
- [12] K.V. Shitikova, et al, Preprint JINR-83-1043, (1983).
- [13] B.G. Harvey, Phys. Rev. C **49**, 2890 (1994).
- [14] I. Tanihata, et al. Phys. Lett. **B206**, 593 (1988).
- [15] I. Tanihata, et al. Phys. Lett. **B287**, 307 (1992).
- [16] I. Sick and J.S. McCarthy, Nucl. Phys. **A150**, 631 (1970).
- [17] J. Li, et al, Nucl. Phys. **A162**, 531 (1971).
- [18] V.V. Burov, et al, J. Phys. G. **7**, 137 (1981).
- [19] B.G. Harvey, Nucl. Phys. **A444**, 498 (1985).
- [20] V.P. Garistov, et al, Sov. J. Nucl. Phys. **55**, 73 (1992).
- [21] O.V. Bepalova, et al, Izv. AN USSR, ser. Phys. **55**, 2257 (1991).
- [22] T. Kobayashi, et al, Phys. Rev. Lett. **60**, 2599 (1988).
- [23] W.R. Gibbs and A.C. Hayes, Phys. Rev. Lett. **67**, 1395 (1991).
- [24] M.C. Mermaz, Phys. Rev. C **47**, 2213 (1993).

TABLES

TABLE I. Classification of the isotopes

$AZ$	$J^\pi$	T	[f]
${}^6\text{Li}$	$1^+$	0	[42]
${}^7\text{Li}$	$3/2^-$	$1/2$	[43] [421]
${}^8\text{Li}$	$2^+$	1	[431] [422]
${}^9\text{Li}$	$3/2^-$	$3/2$	[432] [4221]
$({}^{10}\text{Li})$	$(1^+)$	2	[4222]
$({}^{10}\text{Li})$	$(2^+)$	2	[4321]
${}^{11}\text{Li}$	$3/2^-$	$5/2$	[4322]
${}^{13}\text{Li}$	$3/2^-$	$7/2$	[43222]
${}^6\text{Be}$	$0^+$	1	[42]
${}^7\text{Be}$	$3/2^-$	$1/2$	[43] [421]
${}^8\text{Be}$	$0^+$	0	[44] [422]
${}^9\text{Be}$	$3/2^-$	$1/2$	[441] [432] [4221]
${}^{10}\text{Be}$	$0^+$	1	[442] [4321] [4222]
${}^{11}\text{Be}$	$1/2^+$	$3/2$	[4331]
${}^{12}\text{Be}$	$0^+$	2	[4431] [4422]
${}^7\text{B}$	$3/2^-$	$3/2$	[421]
${}^8\text{B}$	$2^+$	1	[431] [422]
${}^9\text{B}$	$3/2^-$	$1/2$	[441] [432] [4221]
${}^{10}\text{B}$	$3^+$	0	[442] [4321] [4222]
${}^{11}\text{B}$	$3/2^-$	$1/2$	[443] [4421] [4322]
${}^{12}\text{B}$	$1^+$	1	[4431] [4422]
${}^{13}\text{B}$	$3/2^-$	$3/2$	[4432]
${}^8\text{C}$	$0^+$	2	[422]
${}^9\text{C}$	$3/2^-$	$3/2$	[432] [4221]
${}^{10}\text{C}$	$0^+$	1	[442] [4321] [4222]
${}^{11}\text{C}$	$3/2^-$	$1/2$	[443] [4421] [4322]
${}^{12}\text{C}$	$0^+$	0	[444] [4422]
${}^{13}\text{C}$	$1/2^-$	$1/2$	[4441] [4432]
${}^{14}\text{C}$	$0^+$	1	[4442]

TABLE II. Calculated binding energies and the rms radii.

$AZ$	$\hbar\omega$ [Mev]	$-E_0$ [MeV]	$-E_{exp}$ [MeV]	$r_{rms}$ [fm]	$1.2A^{1/3}$ [fm]
${}^6\text{Li}$	19.47	30.1	30.5	2.41	2.18
${}^7\text{Li}$	19.71	38.0	37.7	2.45	2.30
${}^8\text{Li}$	16.44	36.1	39.7	2.57	2.40
${}^9\text{Li}$	16.21	42.4	43.8	2.63	2.50
${}^{11}\text{Li}$	13.68	48.1	44.1	2.76	2.67
${}^{11}\text{C}$	16.01	72.3	70.4	2.61	2.67

TABLE III. Parameters and rms radii for each shell, in fm.  $r_o$  stands for the parameters of the outer/halo neutrons.  ${}^{11}\text{Li}_p$  has four of them close to the p-shell; for  ${}^{11}\text{Li}_h$  two neutrons are on the p-shell, and another two are loosely bound halos.

$AZ$	$r_A$	$r_p$	$r_o$	$\sqrt{\langle r^2 \rangle_s}$	$\sqrt{\langle r^2 \rangle_p}$	$\sqrt{\langle r^2 \rangle_o}$	$\sqrt{\langle r^2 \rangle_{tot}}$
${}^6\text{Li}$	1.46	1.52		1.84	2.50		2.09
${}^{11}\text{Li}_p$	1.74	1.93	2.77	2.18	2.95	4.48	3.14
${}^{11}\text{Li}_h$	1.74	1.93	1.93	2.18	2.95	2.95	3.14
halo			3.28			5.23	
${}^{11}\text{Be}$	1.64	1.75	2.63	2.05	2.81	4.26	2.86
${}^{11}\text{C}$	1.60	1.71		2.01	2.76		2.52
${}^{12}\text{C}$	1.61	1.77		2.02	2.86		2.61
${}^{12}\text{C}$ Eq. (31)	2.0	1.70		2.45	2.68		2.61

TABLE IV. Experimental and calculated total reaction cross section  $\sigma_R$  and inclusive cross section  $\sigma_{11C}$  for the reaction  $^{12}\text{C} + \text{C}$ , 1000 MeV/A.  $\sigma_B$  and  $\sigma_N$  are the widths of the broad and narrow momentum components. Cross sections are in mb.

	$\sigma_B$	$\sigma_N$	$\sigma_R$	$\sigma_{11C}$
Experiment	105		930	47
Ref. [13]	96	36	929	61
$n(R_{0K})$	87	53	943	65
$n(\chi)$	96	40	937	63
n(Eq.31)	113	45	929	48

TABLE V. Comparison of transverse momentum widths for  $^9\text{Li}$  fragments, experimental and calculated total reaction cross section and inclusive cross sections for the reaction  $^{11}\text{Li} + \text{C}$ , 790 MeV/A.  $\sigma_B$  and  $\sigma_N$  are the widths of the broad and narrow momentum components.  $B/N$  is the ratio of their areas. Cross sections are in mb.

	$\sigma_B$	$\sigma_N$	$B/N$	$\sigma_R$	$\sigma_{9Li}$	$\sigma_{8Li}$	$\sigma_{8He}$
Experiment	80	21	1.5	1042	213	62	26
Ref. [13]	80	21	1.22	1036	180	54	30
$n(^{11}\text{Li}_h)$	80	28	1.65	994	147	48	30
$n(^{11}\text{Li}_p)$	82	34	1.75	978	147	37	25

TABLE VI. Comparison of  $^{11}\text{Li}$ ,  $^{11}\text{Be}$  and  $^{11}\text{C}$  projectiles on a standard  $^{12}\text{C}$  target. All cross-sections are in mb.

$AZ$	$\sigma_R$	$\sigma_R(\text{exp})$	Ref. [24]
$^{11}\text{Li}$	994	1042	
$^{11}\text{Be}$	946	942	
$^{11}\text{C}$	884		800.6

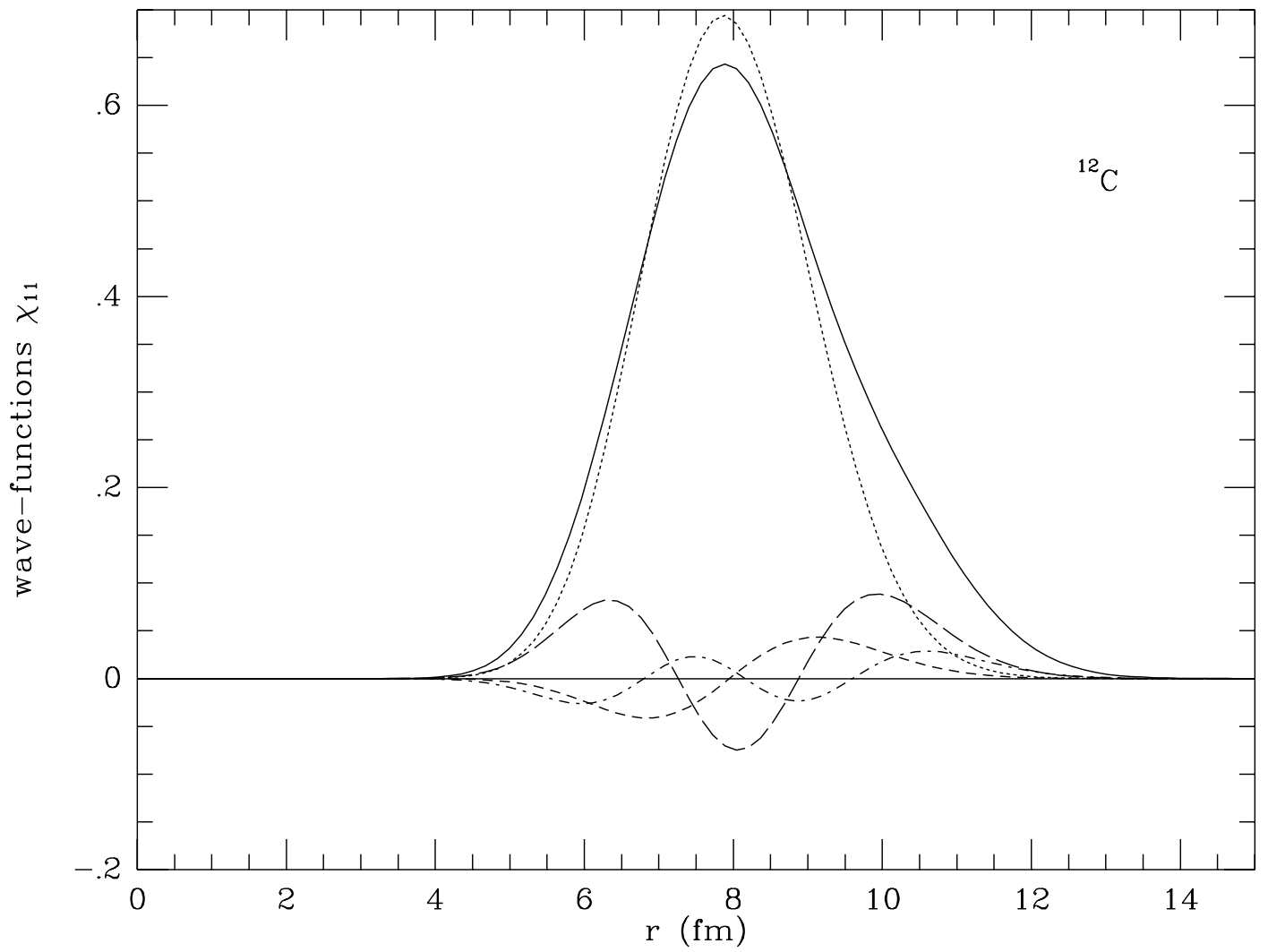


Figure 1: The wave function (solid line) and its components.

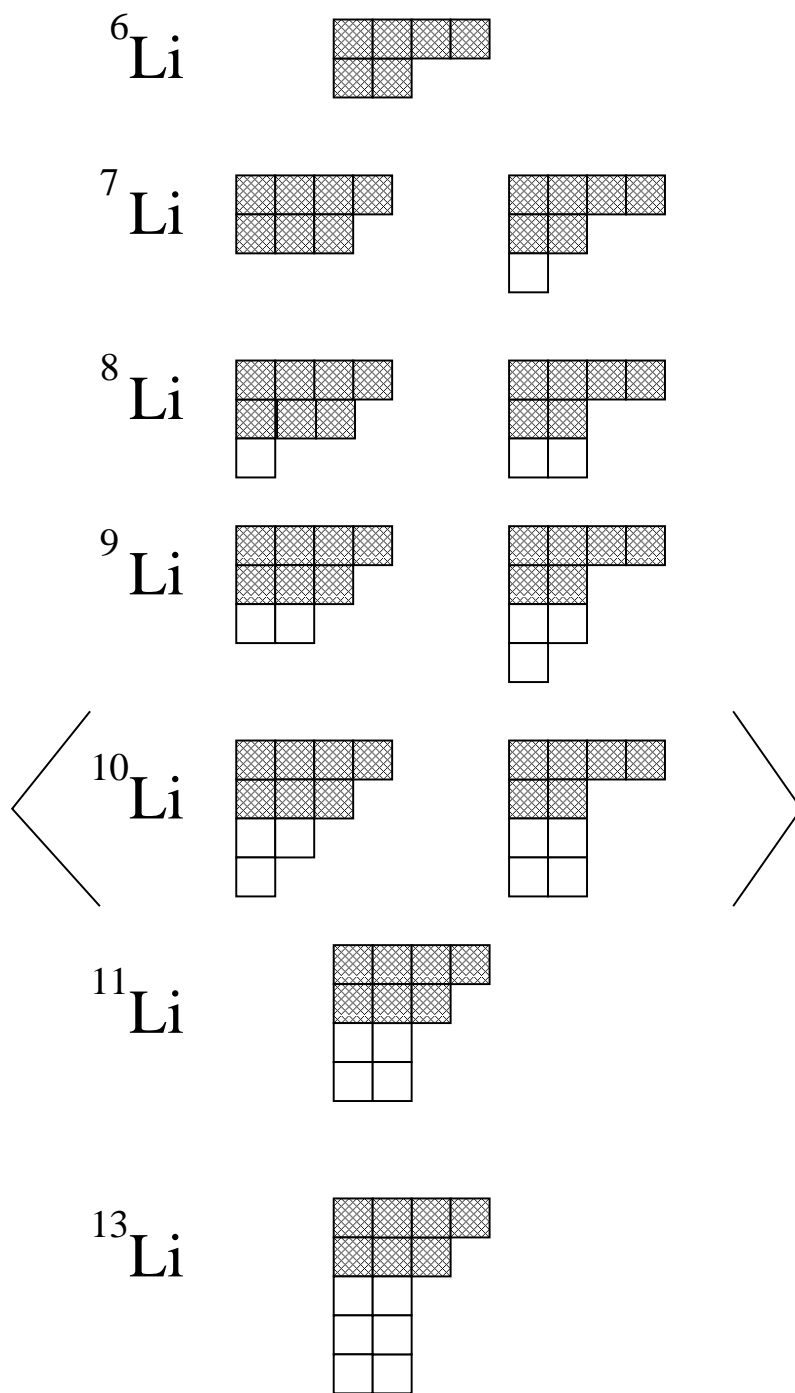


Figure 2: Young Diagrams for Lithium isotopes.

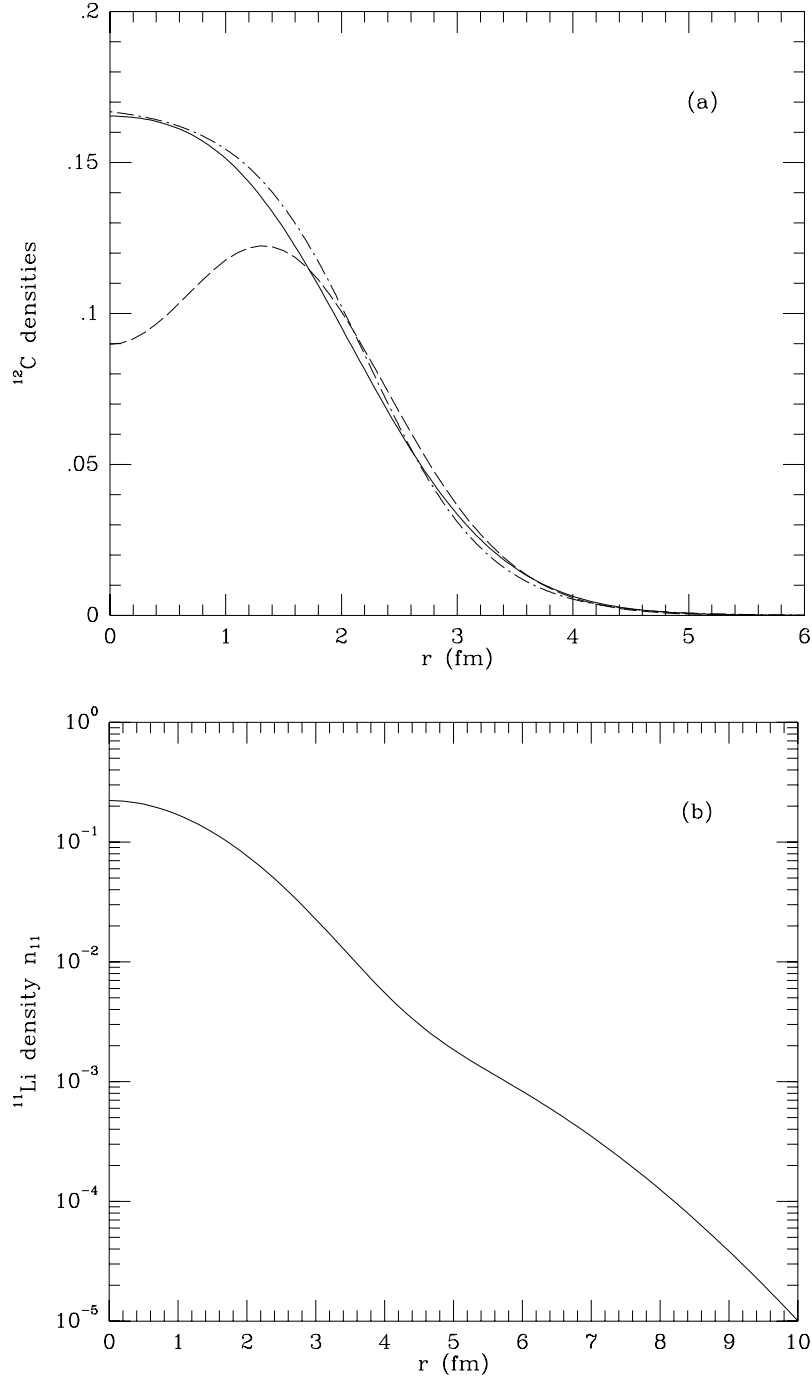


Figure 3: (a) The HSF density distribution for  $^{12}\text{C}$  (solid line) as compared to the Eq. (31) approximation (dashed) and phenomenological one (dot-dashed) from Ref. [13]. (b) The HSF density for  $^{11}\text{Li}$ .



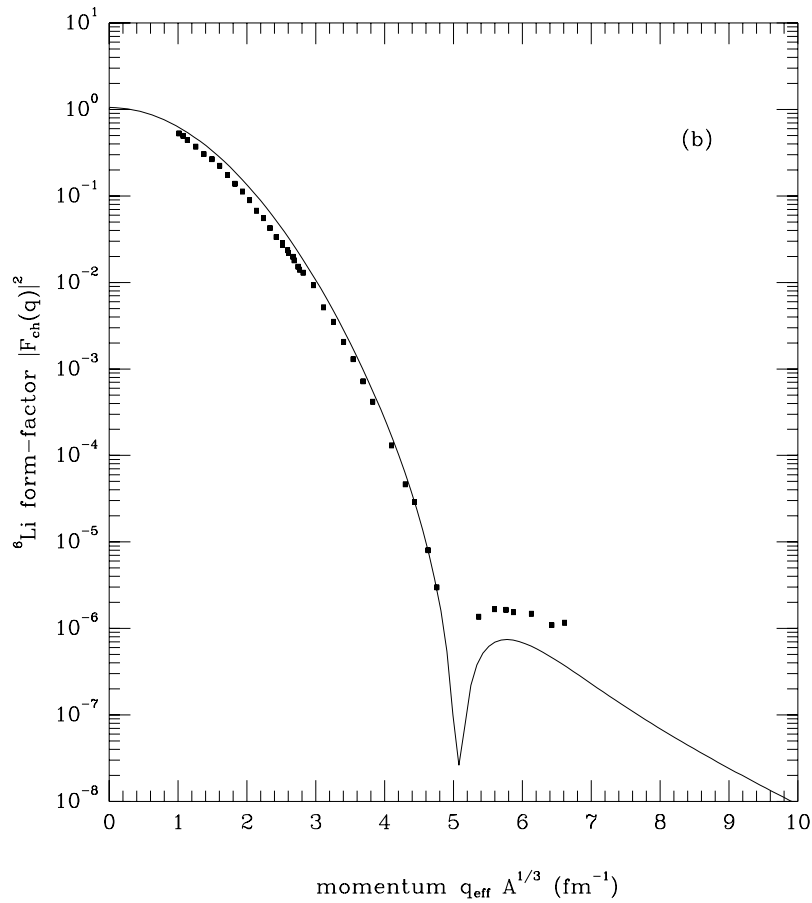
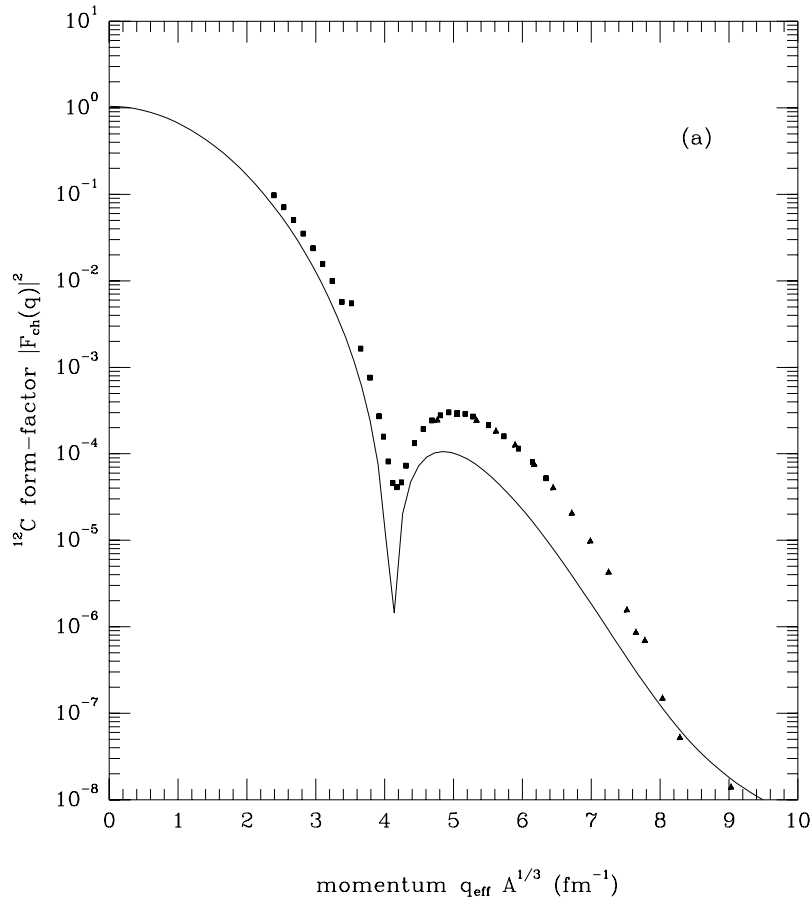


Figure 4: The charged form-factors for (a)  $^{12}\text{C}$  and (b)  $^6\text{Li}$ . Experimental points are taken from Refs. [16] and [17] respectively.

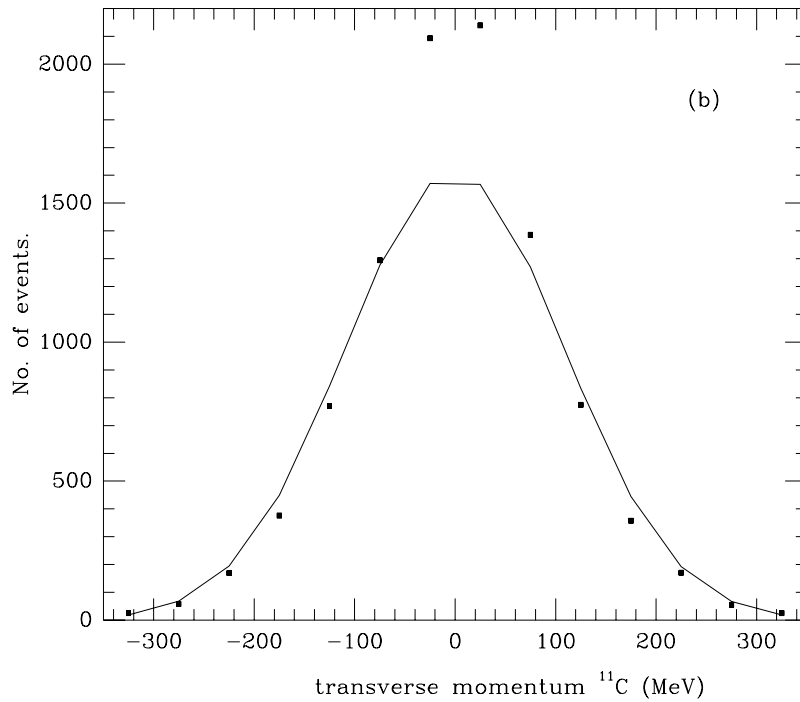
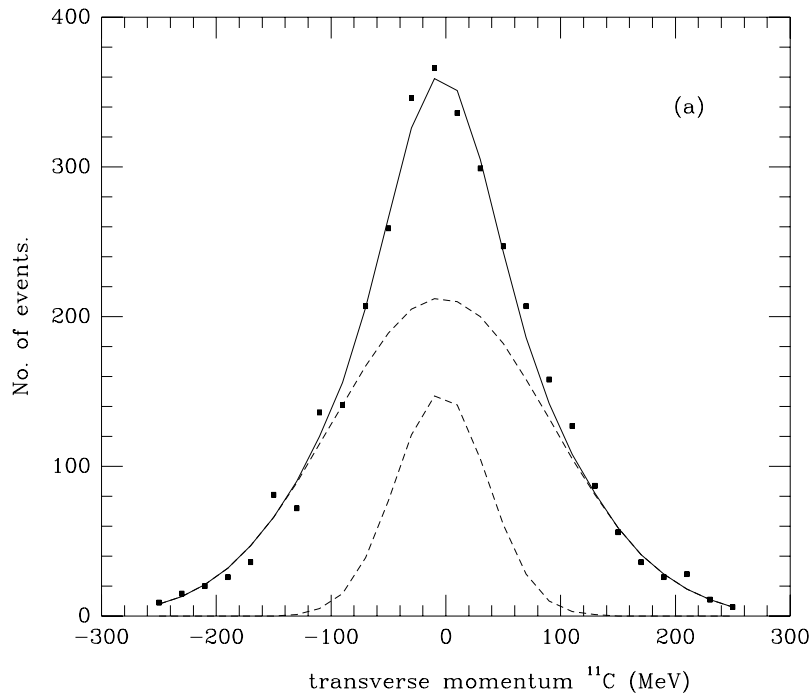


Figure 5: (a) Transverse momentum distribution of  $^{11}\text{C}$  fragments from the reaction  $^{12}\text{C} + \text{C}$ , 1 GeV/nucleon. Filled squares are the calculated points, with a bin size 20 MeV/c. Dashed lines are least squares fit to the broad and narrow momentum components. (b) Fit to the calculation of (a) with a single Gaussian, with a bin size 50 MeV/c, similar to experiment.

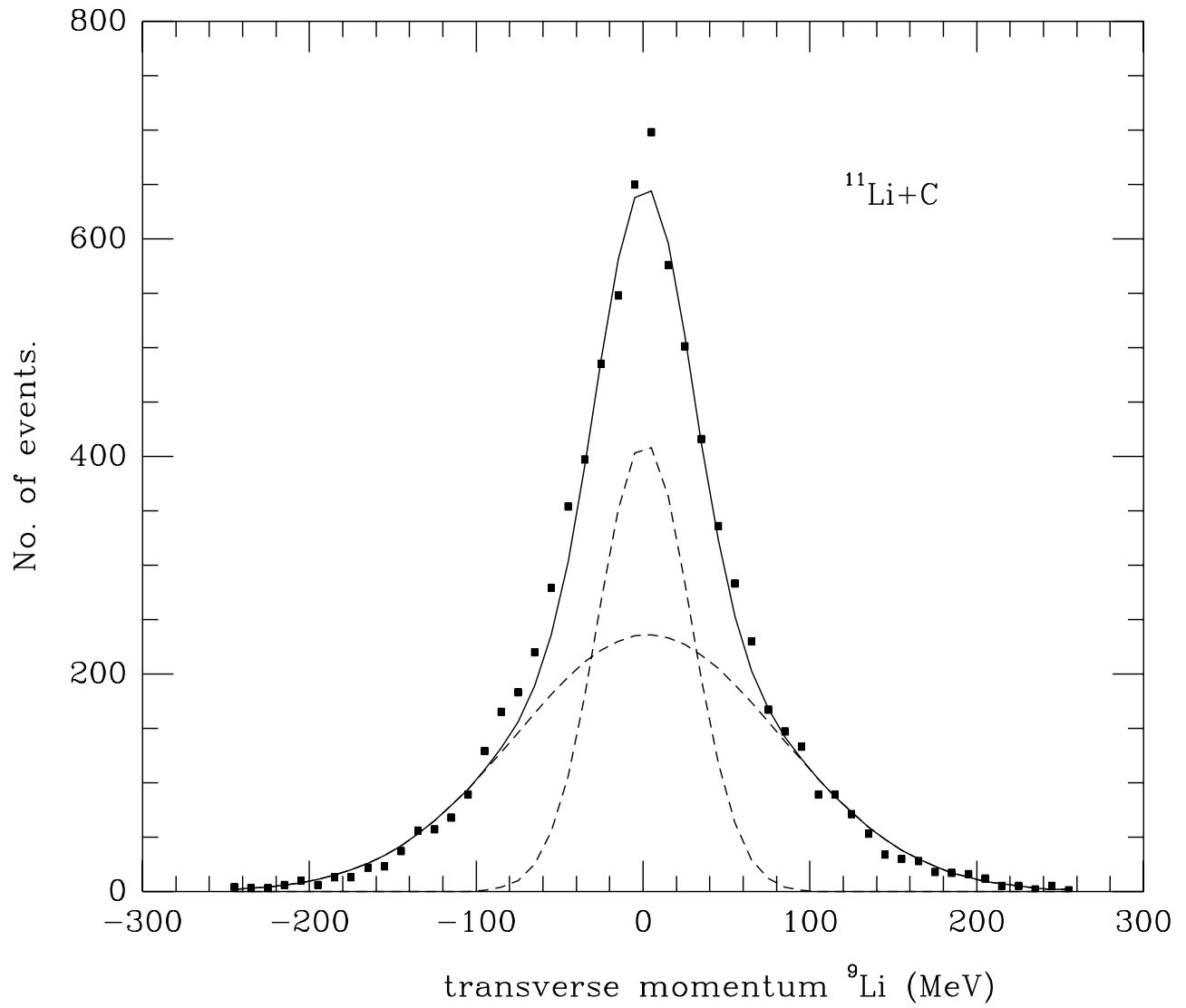


Figure 6: The same as Fig. 5, for  ${}^9\text{Li}$  fragments from the reaction  ${}^{11}\text{Li} + \text{C}$ , 790 MeV/nucleon.